A Chip-Scale Optical Frequency Reference for the Telecommunication Band Based on Acetylene

*Roy Zektzer, Matthew T. Hummon, Liron Stern, Yoel Sebbag, Yefim Barash, Noa Mazurski, John Kitching, and Uriel Levy**

Lasers precisely stabilized to known transitions between energy levels in simple, well-isolated quantum systems such as atoms and molecules are essential for a plethora of applications in metrology and optical communications. The implementation of such spectroscopic systems in a chip-scale format would allow to reduce cost dramatically and would open up new opportunities in both photonically integrated platforms and free-space applications such as lidar. Here the design, fabrication, and experimental characterization of a molecular cladded waveguide platform based on the integration of serpentine nanoscale photonic waveguides with a miniaturized acetylene chamber is presented. The goal of this platform is to enable cost-effective, miniaturized, and low power optical frequency references in the telecommunications C band. Finally, this platform is used to stabilize a 1.5 μm laser with a precision better than 400 kHz at 34 s. The molecular cladded waveguide platform introduced here could be integrated with components such as on-chip modulators, detectors, and other devices to form a complete on-chip laser stabilization system.

1. Introduction

Frequency stabilized lasers are in great demand for a variety of applications such as atomic clocks,[1–5] dimensional metrology,[6] spectrum analysis,[7] dense wavelength division multiplexing (DWDM) systems,[8,9] and the realization of the meter.[10,11] Alkali atomic vapors such as rubidium[12] and cesium have reasonably narrow (≈6 MHz) optical transition linewidths in the near-infrared, high room-temperature vapor pressures, and large absorption cross-sections that result in optical detection with high signal-to-noise ratio. The optical frequency of the D2 transition of ^{87}Rb at 780 nm has been measured to a relative standard uncertainty of 5×10^{-10} and is recommended by the Bureau International des Poids et Mesures (BIPM) as a practical realization of the SI meter.

In the past few years we have observed immense progress toward the goal of integrating and miniaturizing atomic vapor cells by the use of integrated nanophotonic–atomic devices such as the atomic cladded waveguide (ACWG),[13,14] atomic cladding microring resonator (ACMRR),[15–17] atomic cladded Mach Zehnder interferometer,[18] coupled plasmonic–atomic and plasmonic molecular devices,[19–21] antiresonant reflecting optical waveguides (ARROW),[22] hollow core fibers,[23,24] or by use of compact anodically bonded rubidium cells.[25,26] While alkali atoms can satisfy the need for stabilized sources in the near infrared frequency regime (e.g., around 780 nm wavelength for rubidium), compact stabilized light sources at the telecom regime are in great demand. Recently, stabilization of a telecom laser at 1560 nm was demonstrated using a photonic chip frequency doubler by using the second harmonic generated at 780 nm to probe the rubidium D2 transition.[27] Additionally, stabilization of a laser at 1529 nm to an excited state transition in rubidium was also demonstrated,[28,29] though in general, the number of telecom reference transitions available in atomic species is limited due to their simple electronic structure.

One approach that allows circumventing this obstacle is the use of molecular transitions. Indeed, gas molecules such as acetylene ($^{12}C_2H_2$)[30] and hydrogen cyanide (HCN)[31] have transitions at the telecom band and are being used as frequency standards. Work has been progressing to integrate $^{12}C_2H_2$ with fiber-based platforms[32–34] and recently on-chip spectroscopy of CH_4 at 1.65 μm was demonstrated in the context of trace gas sensing.[35] A primary challenge in implementing molecular spectroscopy in more compact geometries is the small absorption cross-sections of most useful molecules (I_2 being a notable exception[36]). The small absorption typically implies the use of high gas pressures, at which significant temperature-dependent collisional shifts to the transition frequencies are present.[30] At lower pressures, accurate stabilization can be achieved, and the C_2H_2 is a recommended practical realization of the meter under these conditions. However, in this case long interaction lengths are required to generate a sufficiently large absorption signal,

R. Zektzer, Y. Sebbag, Dr. Y. Barash, N. Mazurski, Prof. U. Levy
Department of Applied Physics, The Benin School of Engineering and Computer Science, The Center for Nanoscience and Nanotechnology
The Hebrew University of Jerusalem
Jerusalem 91904, Israel
E-mail: ulevy@mail.huji.ac.il

Dr. M. T. Hummon, Dr. L. Stern, Prof. J. Kitching
Time and Frequency Division
National Institute of Standards and Technology
325 Broadway Boulder, CO 80305, USA

The ORCID identification number(s) for the author(s) of this article can be found under https://doi.org/10.1002/lpor.201900414

DOI: 10.1002/lpor.201900414

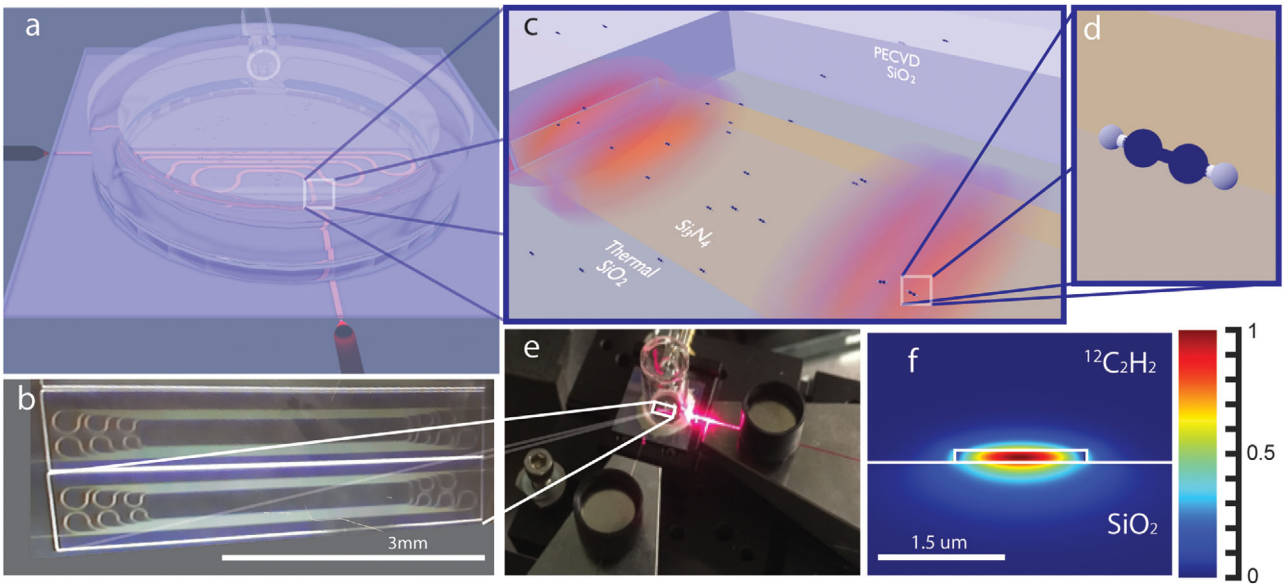

Figure 1. a) Measurement and device scheme: light is focused by a lensed fiber to the MCWG, propagates through a serpentine shape waveguide and collected by another lensed fiber. b) Microscope image of two swirl waveguides. c) Schematic of the interaction region: The optical mode propagates in the exposed region where the oxide is etched and interacts with the moving gas molecule. d) Schematic of C_2H_2 molecule. e) Photograph of the MCWG device and f) cross section of the normalized electric field distribution of the TE mode.

with the light sometimes confined in optical cavities.[37] If these challenges can be overcome, the acetylene $\nu_1 + \nu_3$ band offers a grid of absorption lines covering most of the telecommunication band highly suitable for the stabilization of WDM lasers. Chip scale integration of frequency stabilization systems offers several prominent opportunities such as significant cost reduction by using well established and scalable fabrication techniques, integration of multiple electro optic devices such as detectors,[38] and phase modulators[39] on the same chip, and even the integration of optical functionalities with the required electronics[40] on the same platform. With such an approach, miniaturized configurations for stabilization of photonic devices such as frequency combs[41] or microring resonators (MRRs)[42] using the integrated reference cells are feasible, broadening the horizons of frequency references. One example addressing the importance of such integration is precise measurement in space,[43,44] for which stabilized laser systems with low payload are highly desired.[45] Another important advantage of this chip scale integrated scheme relates to the ability to confine light at the nanoscale, which may give rise to the observation of nonlinear phenomena in atoms[15,46,47] and molecules using relatively low levels of optical power while maintain high optical density in the confined mode. For instance, while preforming saturated absorption spectroscopy or observing electromagnetic induced transparency (EIT) may be a challenging task in low dipole gases such as acetylene, the strong light confinement may allow the observation of such effects, as was shown in hollow core photonic crystal fibers filled with acetylene.[48–50] On-chip waveguides also critically allow for long optical path lengths to be achieved in a small volume with serpentine waveguides,[35,51] resulting in increased optical absorption and improved signal.

Motivated by the grand vision of fabricating a full on-chip stable and accurate locking system, we have designed, fabricated, and experimentally demonstrated the chip scale integration of acetylene with optical waveguides to construct a molecular cladded waveguide (MCWG). We have observed for the first time the spectroscopic acetylene absorption lines using light guided by a nanophotonic structure. High contrast of about 10% was achieved owing to the long propagation length of about 4 cm. By designing the waveguide to take a serpentine shape, the physical device volume is as small as 5×10^{-3} mm^3 (3 mm × 0.4 mm × 4 µm). Finally, we have demonstrated the usefulness of the MCWG platform for practical applications by stabilizing a laser to 1.6×10^{-9} in fractional frequency, corresponding to a precision of better than 400 kHz at 34 s. While these results are already sufficient for current DWDM systems[8,9] and distance measurements at high resolution,[52] further stability enhancement can be achieved, as discussed in the conclusion section. Moreover, the use of guided wave platform offers a true opportunity for dense integration of multiple functionalities on chip, allowing to scale up the demonstrated platform toward compact, cost effective, and multichannel stabilization systems.

2. MCWG Platform

Our MCWG platform is illustrated in **Figure 1**a. Our device consists of a 40 mm long silicon nitride (Si_3N_4) core waveguide on top of a SiO_2 cladding layer (Figure 1b). Light is coupled on and off the chip using a pair of lensed optical fibers. The waveguide cross-section is 1.5 µm width by 0.25 µm height, the waveguide is covered with 2 µm thick SiO_2 layer, serving as an upper cladding. A buffered hydrofluoric acid (HF) wet etch is used to remove the upper oxide layer to expose the waveguide over a predefined area, which serves as the interaction region between the molecular gas and the optical mode (Figure 1c). A glass cap is

then bonded to the chip. Next, the device is evacuated, filled with $^{12}C_2H_2$ (Figure 1d) and pinched off, resulting in a portable, hybrid molecular–photonic device as shown in Figure 1e. We have chosen silicon nitride for a few reasons. 1) Si_3N_4 is transparent from ≈300 nm to ≈6.5 µm making it suitable for acetylene transitions in the telecom, near IR, and mid IR. 2) In order observe nonlinear phenomena in acetylene such as saturated absorption spectroscopy or EIT, high intensities are required.[50] Unlike silicon, the large bandgap of Si_3N_4 prevents undesired two photon absorption which may lead to extreme temperatures. 3) Furthermore, avoiding two photon absorption supports the observation of high Q factor resonators at decent intensities.[51,53] Such resonators can be used to extend the frequency stability of the acetylene transition to other wavelength through nonlinear effects such as harmonic generation and four-wave mixing. The transverse electric (TE) optical mode supported by the waveguide is presented in Figure 1f where ≈10 % of the field extends into the acetylene region and interacts with it. The interaction of light with the acetylene molecules in our system is modelled by calculating the susceptibility of a quantum emitter that is reflected from a surface in the presence of a decaying electromagnetic field, following refs. [13,54]. This model results in a Voight-like absorption profile. Three major broadening mechanisms are present in our system that affect the acetylene absorption linewidth: 1) Doppler broadening, defined as $\Delta\omega = k_z \cdot v_{Ac}$, where v_{Ac} (430 m s^{-1}) is the most probable velocity of acetylene at room temperature (295 K) and k_z is the wave number of the mode along the propagation direction. 2) Pressure broadening, estimated as $\Delta\omega = P$ [Torr] ·13 [MHz Torr^{-1}].[55] In our system the pressure of acetylene is 30 Torr and hence the pressure broadening is estimated to be about 390 MHz. 3) Transit time broadening, which is the result of the finite interaction time between the molecule and the waveguide evanescent field that is confined at the nanoscale, thus giving rise to additional spectral broadening. The evanescent decay length is deduced from the mode wavenumber in the transverse direction. We have modeled the optical mode by using finite element method (FEM) simulation and found the effective index of the mode to be 1.5 and the evanescent decay length to be about 0.2 µm. In order to assess the effect of acetylene on the mode effective index we have assumed a small imaginary index of 10^{-4} for the cladding of the waveguide and calculated the mode effective imaginary index, which was found to be ≈10^{-5}. This indicates an interaction factor (IF) of 10%. Having the mode wave vector in hand, we have simulated the refractive index of acetylene and found the linewidth to be ≈1100 MHz. This broad linewidth is a result of an increased Doppler broadening and increased transit time broadening. The expected Doppler width in a free space system is ≈480 MHz.[56] In contrast, the simulated Doppler width for the MCWG based system is ≈700 MHz. The Doppler broadening in the MCWG is increased by ≈50% compared to the free space measurement as it is proportional to the photon momentum. Given the fact that the photons are propagating as confined mode having an effective index of about 1.5, the wavenumber and hence the momentum are also increasing by 50% as compared to free space.

In addition to the enhanced Doppler broadening, we estimate the transit time broadening to be ≈160 MHz due to the finite time it takes for the molecule to cross the evanescent tail of the optical beam. Taking into account these broadening mechanisms we can extract the complex refractive index of acetylene which is tied to the optical mode. Once the complex refractive index of the acetylene is known, we calculate the expected device transmission (T), according to the Beer–Lambert law following the relation $T = \exp(-2\cdot k\cdot L\cdot \mathrm{IF})$, where L is the propagation length and $k = 2\pi \cdot n_i/\lambda$ (n_i being the imaginary part of the refractive index of the acetylene and $\lambda = 1520$ nm)

A more detailed explanation of this calculation is provided in the Supporting Information.

3. Results

In **Figure 2**a,b we plot the transmission measured from our MCWG device and from a $^{12}C_2H_2$ reference cell over a broad spectral range of about 4.5 nm around the telecom band. This measurement was carried out with a coarse scanning of our tunable telecom laser (HP 81682A). We have normalized the device transmission to remove the effects of Fabry–Perot etalons; these fluctuations will be discussed in detail in the Supporting Information.

We have also performed a finer scan over a single absorption line of the R9 transition, as can be seen in Figure 2c. Here, we plot the measured and the calculated transmission through our device (30 Torr, red and dashed green, respectively). The method of calculated transmission is briefly explained in the text. A more detailed explanation is provided in the Supporting Information. As a reference, we also plot the transmission through our device using a free space beam by illuminating it through the epoxy bonded glass cup that is attached to the chip. The free space beam has a waist of ≈1 mm and it propagates 0.5 cm above the chip with a power of 1 mW. As can be seen (Figure 2c) there is a good agreement between the simulation and the measurement, where both show absorption linewidth of about 1.1 GHz. The 4 cm long propagation length results in 10% contrast as can be seen in Figure 2c. The only free parameter in the simulation is the optical density due to small uncertainty in the waveguide dimensions and in the transition dipole strength, which we have extracted by measuring the transmission from a 5 cm long reference cell. The variation of the free parameter was less than 10%. One can also see that the reference absorption line is narrower, mostly due to the reduced Doppler broadening. Details about the extraction of the simulated curve are given in the Supporting Information. We couple light to the device by using inverse tapers. We estimate the coupling losses to be ≈3 dB per facet. The total loss of the device is ≈40 dB, most of the loss is due to fabrications imperfections such as write fields misalignment. Assuming symmetrical losses, the optical power within the waveguide is found to be ≈100 nW. The saturation intensity of the acetylene transition is ≈4×10^8 W cm^{-2},[55] and the mode size supported by our waveguide is 1.5×0.25 µm^2. This results in an intensity of about ≈27 W cm^{-2}. For such intensity it is reasonable to neglect power broadening. Next, we demonstrate the capability of our platform to perform as a chip scale frequency reference. The locking scheme used for this purpose is presented in Figure 3a, where a tunable laser at a telecom wavelength is locked by a wavelength modulation scheme[57] to the MCWG absorption line ($^{12}C_2H_2$, R9) at 1520.08 nm. We compare its stability to a second laser that is locked to the R29 absorption line of a reference cell ($^{13}C_2H_2$) at

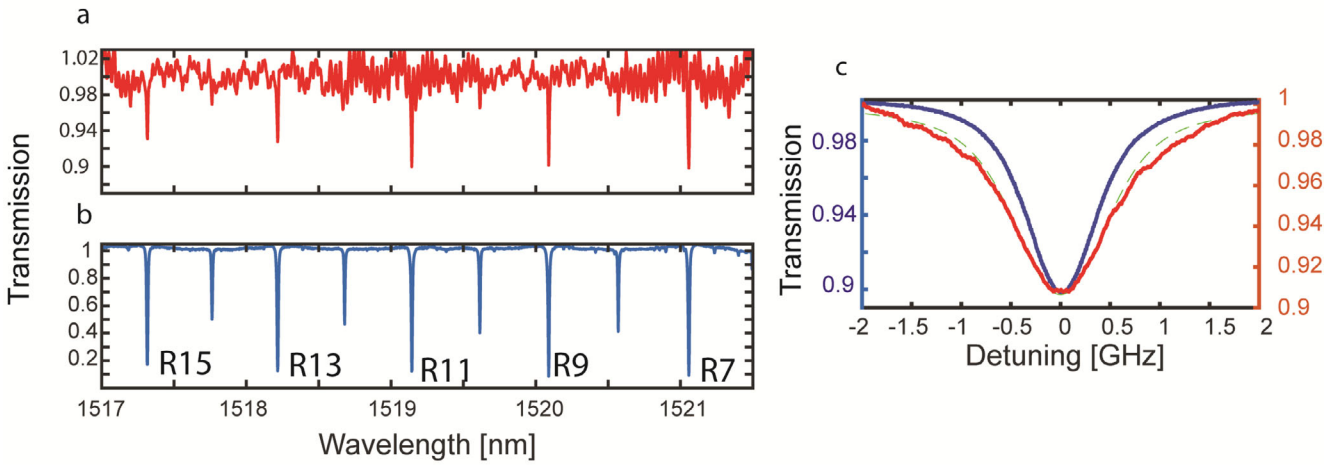

Figure 2. a) Measured light transmission from our MCWG. b) Measured light transmission from a reference cell. c) Measurement of the R9 transition from our MCWG (red line and right red axis) and a reference cell (blue line and left blue axis). Simulation showing the expected transmission spectrum of our MCWG is shown in dashed green

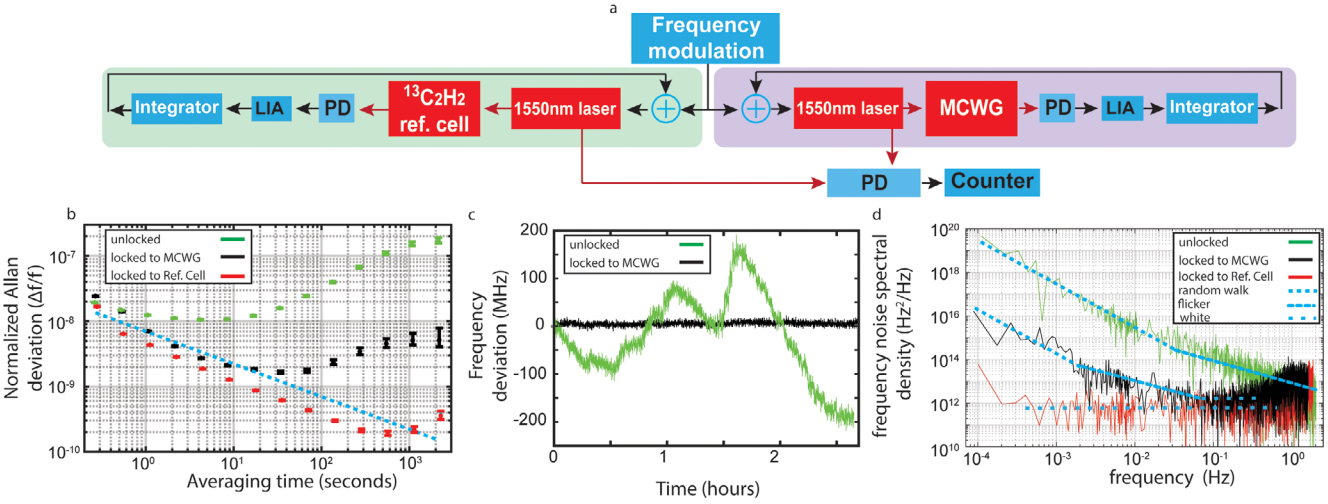

Figure 3. a) Locking scheme: Two lasers at 1550 nm are locked to acetylene absorption lines, one obtained from a reference cell and the other from our MCWG. The beating signal between the two lasers is fed into a counter, which extracts the beating frequency. LIA, lock-in amplifier and PD, photodetector. b) Allan deviation extracted from the beating between a laser locked to a reference cell and: free running laser (green), laser locked to another reference cell (red) and laser locked to our MCWG (black). The error bars represent a confidence interval of 0.683. The blue dashed line represents the Shot noise limited stability ($7 \times 10^{-9}/\sqrt{\tau}$). c) Time series of laser instability for the unlocked (green) and locked (black) laser. d) Frequency noise spectral density of: free running laser (green), laser locked to another reference cell (red), and laser locked to our MCWG (black). The dashed lines represent the different noise regions.

≈1520.08 nm with a contrast of 5%. The two transitions ($^{12}C_2H_2$, R9, $^{13}C_2H_2$, R29) are ≈3.2 GHz apart. We have measured the beat signal between the two lasers and extracted the frequency instability given by the Allan deviation, as shown in Figure 3b (black points). For comparison, we have also measured the instability between two lasers both locked to reference cells (red points) and the instability of a free running laser (green points). The results show that our device can provide laser stabilization to the level of 1.6×10^{-9} at 34 s. As shown, this result is significantly better than the stability of our free running laser, and only one order of magnitude inferior to the stability obtained with the large reference cell. In **Figure 3**c we plot the beating signal as a function of time of the locked laser (black) and the unlocked laser (green). While the free running laser can have drift of 300 MHz in an hour, the locked laser is much more stable. In Figure 3d we plot the frequency noise spectral density. We are able to reduce the flicker noise of the laser at short time scales of few seconds. At longer times, corresponding to lower frequencies of 10^{-2} Hz, the laser which is locked to our MCWG (black) absorption signal suffers from flicker noise. This noise is not observed in the reference cell system (red) and thus is not attributed to electrical noise (which should be identical in both feedback systems). Our results show significant reduction in random walk noise as compared to the case of free running laser.

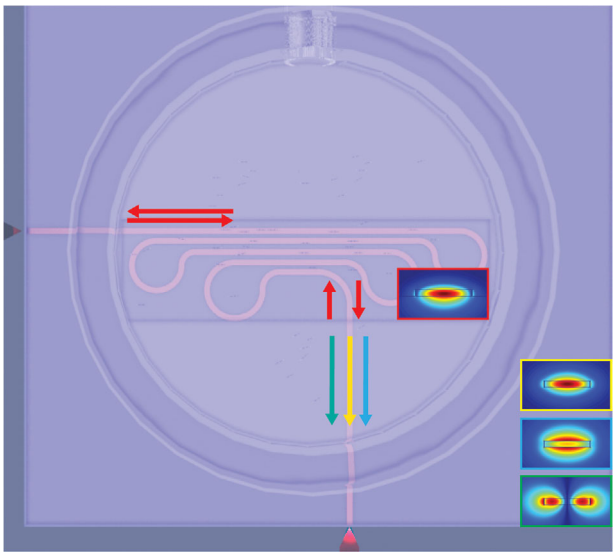

Figure 4. Schematic of the device and mode propagation: in the interaction area there is a single mode that will reflect at the facets (red arrows). This mode will couple to the three modes in the coupling waveguide (green, yellow, and blue arrows).

4. Discussion

We have developed and demonstrated the platform of MCWG consisting of a silicon nitride waveguide integrated with a microscopic acetylene cell. The measured transmission spectrum through the device shows distinct absorption lines of acetylene. We have further shown (Figure 3) that our integrated device can be used to stabilize a laser to a precision of better than 400 kHz at 34 s. This result is an order of magnitude improvement compared to the stability of our free running laser. The improvement becomes even larger at longer integration times. The current level of instability is attributed to two major reasons: 1) fluctuation in the coupling conditions between the external fibers to the device, and 2) fluctuations in temperature. Our current version of the MCWG device consists of two different sections (**Figure 4**): the coupling region, which is covered with SiO_2, and the interaction region, where the SiO_2 cladding is etched off. While the interaction region (which is contained within the rectangle in Figure 1b,c) is a single mode waveguide, the coupling waveguide supports both the fundamental TE (Figure 4, yellow arrow) and the transverse magnetic (TM) (Figure 4, green arrow) mode as well as an additional TE mode (Figure 4, blue arrow). Therefore, as the coupling conditions vary over time due to mechanical shift of the external fibers, the beating between the modes varies over time, affecting the measured transmission spectrum. Furthermore, reflections from the boundaries between the two different waveguide regions (having different mode profiles and different mode effective indices) and from defects resulting from the imperfections generated during the fabrication process, all may result in Fabry–Perot (FP) resonances, corresponding to forward and backward propagating modes, denoted by the red arrows in Figure 4. As previously reported,[15,19,21] such effects may result in a spectral shift in the transmission dip due to the Fano effect, as well as variations in the measured intensity at a given frequency. Furthermore, as a result of temperature variations, such FP resonances can shift in frequency due to the thermo optic effect. To estimate the expected effect of such phenomena on the measured signal, we have simulated the transmission through our device in varying conditions, as explained in more detail in the Supporting Information. These simulations predict spectral shifts of hundreds of kilohertz and even more for our operating conditions. The accuracy of our system is limited by the coupling conditions variations. The beating between the photonic modes is affected by the coupling conditions and this parameter seems to be the one which is affecting the obtained accuracy the most. To verify this hypothesis, we have slightly shifted the lensed fiber which couples light into our device. As a result, we observed up to 20 MHz shift in the beating frequency. Additional parameters which may affect the stability of our system are expected to be less dominant. For example, power fluctuations in the waveguide may also result in FP resonances shift in frequency due to the Kerr effect. However, considering the Kerr effect coefficient (n_2) in Si_3N_4 of 2.45×10^{-15}cm^2 W^{-1},[58] a refractive index change of less than 10^{-13} is expected at typical light intensities within the waveguide. For such a case, this effect is ≈8 orders of magnitude weaker than the thermo optic effect and thus can be neglected. Power fluctuation in the waveguide may also affect stability due to light shift, which was reported to be around 0.25 kHz (W cm^{-2})$^{-1}$ in acetylene. In short times (i.e., seconds), we observe power fluctuations of about 0.2% (≈0.05 W cm^{-2}) resulting in frequency fluctuations significantly below kHz. Even at longer time scales (hours), were the intensity variation are in the order of up to 10 W cm^{-2}, the resulting shift is about 2.5 kHz. Another parameter which may hamper stability is pressure shift, which was reported to be around 300 kHz Torr^{-1}[56] in Acetylene. First, we have verified the absence of leaks in our device by measuring it several times over the period of more than a year. Indeed, we could not observe any reduction in contrast or change in the linewidth of the signal. Yet, in addition to leaks, temperature (T) fluctuations may also generate pressure fluctuations, which in turn resulting in line shift ($\Delta\nu$) according to: $\Delta\nu(T) = \Delta\nu(T_m)\sqrt{T/T_m}$,[56] where T_m is the reference temperature. Our system has a drift of about 1–2 K over 12 h, resulting in a shift of ≈50 kHz.

Temperature shift, coupling shift and power shift are noise source that are most relevant at long time. In contrast, at short time scales the system is expected to be limited mostly by Shot noise. The current in our detector was ≈0.5 pA and the detector bandwidth is 750 Hz, this results in a current shot noise of about 35 fA. Shot noise limited system instability can be described by the expression $\Delta\nu/\nu = 0.2/(\mathrm{SNR}\cdot Q)$,[59] where SNR is the signal to noise ratio and Q is the quality factor of the transition. The acetylene transition has a Q factor of 2×10^5 resulting in instability of $7 \times 10^{-9}/\sqrt{\tau}$, fitting our experimental data.

Another noise factor results from our wavelength modulation locking scheme, adding about ≈10 MHz frequency shift at ≈700 Hz modulation frequency. Considering this as a white noise, the wavelength modulation scheme can be characterized by an instability of about $0.2 \times 10^{-9}/\sqrt{\tau}$.

Finally, the modulation of the laser and the additional signal slope coming from the FP will result in false error signal (also known as amplitude-modulated (AM) noise). As a result,

variation in optical power at the detector are translated to variations in voltage offset supplied to the laser. We have measured the frequency shift due to power fluctuations inside the waveguide to be up to 5 MHz/50 nW. As such, 50% reduction in optical power will result in a 5 MHz shift in the laser frequency. At short times of several minutes our power fluctuations are smaller than 0.2%, resulting in instability of $\approx 10^{-10}$. The coupling conditions from the fiber to the chip over longer times (hours) can drift significantly and cause a more severe shift. This should be improved in future devices.

To conclude, based on our results, simulations and noise assessments, it seems that at short times our system is shot noise limited, whereas at longer integration times the system is limited by temperature and coupling fluctuations and drifts, affecting the FP spectrum. These fluctuations manifest in flicker and random walk frequency noise as presented in Figure 3d. While our simulations may not represent quantitatively the scenario of our device, one can clearly understand the negative role that FP resonances and multimode beating can have on our frequency stability. Therefore, future work will be focused on eliminating the interference effects by designing both sections of the waveguide to be single mode. Furthermore, we will improve the coupling stability by permanently attaching the fibers to the waveguide, e.g., following the approach reported in ref. [26] where fibers were glued to the chip. Finally, we will enhance the temperature stabilization of the apparatus by using a better control system and a larger thermal mass. By doing so, one may expect to obtain a significantly better stabilization. Reducing the noise is one method to improve our system stability. We can improve our quality factor by reducing the pressure and as a result the pressure broadening. Reducing the pressure will reduce the density of the gas and the absorption signal. In order to improve our signal we can increase our interaction length. It was demonstrated that silicon and silicon nitride waveguides can have losses less than 1 dB m^{-1},[60,61] and with sophisticated dense fabrication[62] we can fabricate longer waveguides and increase our signal.

While our current stability of 1.6×10^{-9} falls short with respect to larger systems based on long (meters) gas cells[63] and long (meters) hollow-core fibers,[32] our device offers good stability alongside with remarkable miniaturization and chip scale integration. In fact, by defining a figure of merit of stability to size ratio, the current demonstration is superior compared with the previous demonstrations. Further improvements such as reduction in the pressure and pressure broadening will allow us to preform Saturation absorption spectroscopy as was demonstrated in other acetylene based reference cells.[63] By doing so, Doppler free narrow lines can be obtained, resulting in further improvement in the stability of our system.

To summarize, we have demonstrated experimentally a new platform based on integration of serpentine nanoscale photonic waveguides with a miniaturized acetylene chamber with the goal of enabling cost-effective, miniaturized, and low power optical frequency references in the telecommunications C band. We have used this platform to stabilize a 1.5 μm laser with a precision better than 400 kHz at 34 s. The use of guided wave platform offers a true opportunity for dense integration of multiple functionalities on chip, allowing to scale up the demonstrated platform toward multichannel stabilization systems.

Supporting Information

Supporting Information is available from the Wiley Online Library or from the author.

Acknowledgements

The authors thank Zach Newman and Alejandra Collopy for their comments on the manuscript. Any mention of commercial products is for information only; it does not imply recommendation or endorsement by NIST. The research was supported by the European Research Council (ERC-LIVIN 648575), and by the Israeli Ministry of Science and Technology.

Conflict of Interest

The authors declare no conflict of interest.

Keywords

frequency references, metrology, molecular physics, nanophotonics

Received: November 27, 2019
Revised: March 16, 2020
Published online: May 11, 2020

[1] S. B. Papp, K. Beha, P. Del'Haye, F. Quinlan, H. Lee, K. J. Vahala, S. A. Diddams, *Optica* **2014**, *1*, 10.
[2] A. D. Ludlow, M. M. Boyd, J. Ye, E. Peik, P. O. Schmidt, *Rev. Mod. Phys.* **2015**, *87*, 637.
[3] Y. Y. Jiang, A. D. Ludlow, N. D. Lemke, R. W. Fox, J. A. Sherman, L.-S. Ma, C. W. Oates, *Nat. Photonics* **2011**, *5*, 158.
[4] S. Zibrov, I. Novikova, D. F. Phillips, A. V. Taichenachev, V. I. Yudin, R. L. Walsworth, A. S. Zibrov, *Phys. Rev. A* **2005**, *72*, 011801.
[5] Z. L. Newman, V. Maurice, T. Drake, J. R. Stone, T. C. Briles, D. T. Spencer, C. Fredrick, Q. Li, D. Westly, B. R. Ilic, B. Shen, M.-G. Suh, K. Y. Yang, C. Johnson, D. M. S. Johnson, L. Hollberg, K. J. Vahala, K. Srinivasan, S. A. Diddams, J. Kitching, S. B. Papp, M. T. Hummon, *Optica* **2019**, *6*, 680.
[6] K. Harding, *Handbook of Optical Dimensional Metrology*, CRC Press, Boca Raton, FL **2016**.
[7] ADVANTEST, Q8384 Optical Spectrum Analyzer, **2001**.
[8] M. Koga, M. Teshima, in *Int. Conf. on Integrated Optics and Optical Fiber Communication (OFC/IOOC)*, Technical Digest Optical Fiber Communication Conf. 1999, IEEE, Piscataway, NJ **1999**, pp. 151-151b.
[9] K. Igarashi, T. Tsuritani, I. Morita, K. Katoh, K. Kikuchi, in Opt. Fiber Commun. Conf./Fiber Opt. Eng. Conf. 2013, OSA, Washington, D.C., **2013**, p. OTu2I.6.
[10] R. Felder, *Metrologia* **2005**, *42*, 323.
[11] F. Riehle, P. Gill, F. Arias, L. Robertsson, *Metrologia* **2018**, *55*, 118.
[12] H. S. Moon, W. K. Lee, L. Lee, J. B. Kim, *Appl. Phys. Lett.* **2004**, *85*, 3965.
[13] L. Stern, B. Desiatov, I. Goykhman, U. Levy, *Nat. Commun.* **2013**, *4*, 1548.
[14] L. Stern, B. Desiatov, N. Mazurski, U. Levy, *Nat. Commun.* **2017**, *8*, 14461.
[15] L. Stern, R. Zektzer, N. Mazurski, U. Levy, *Laser Photonics Rev.* **2016**, *10*, 1016.
[16] R. Ritter, N. Gruhler, W. H. P. Pernice, H. Kübler, T. Pfau, R. Löw, *New J. Phys.* **2016**, *18*, 103031.

[17] L. Stern, U. Levy, *Opt. Express* **2012**, *20*, 28082.
[18] R. Ritter, N. Gruhler, W. Pernice, H. Kübler, T. Pfau, R. Löw, *Appl. Phys. Lett.* 041101, **2015**, *107*.
[19] L. Stern, M. Grajower, U. Levy, *Nat. Commun.* **2014**, *5*, 4865.
[20] S. A. Aljunid, E. A. Chan, G. Adamo, M. Ducloy, D. Wilkowski, N. I. Zheludev, *Nano Lett.* **2016**, *16*, 3137.
[21] R. Zektzer, L. Stern, N. Mazurski, U. Levy, *Optica* **2018**, *5*, 486.
[22] W. Yang, D. B. Conkey, B. Wu, D. Yin, A. R. Hawkins, H. Schmidt, *Nat. Photonics* **2007**, *1*, 331.
[23] S. Ghosh, A. R. Bhagwat, C. K. Renshaw, S. Goh, A. L. Gaeta, B. J. Kirby, *Phys. Rev. Lett.* **2006**, *97*, 1.
[24] A. Lurie, P. S. Light, J. Anstie, T. M. Stace, P. C. Abbott, F. Benabid, A. N. Luiten, *Opt. Express* **2012**, *20*, 11906.
[25] W. Loh, M. T. Hummon, H. F. Leopardi, T. M. Fortier, F. Quinlan, J. Kitching, S. B. Papp, S. A. Diddams, *Opt. Express* **2016**, *24*, 14513.
[26] M. T. Hummon, S. Kang, D. G. Bopp, Q. Li, D. A. Westly, S. Kim, C. Fredrick, S. A. Diddams, K. Srinivasan, V. Aksyuk, J. E. Kitching, *Optica* **2018**, *5*, 443.
[27] J. Xie, J.-Q. Wang, Z.-B. Wang, X.-X. Hu, X. Guo, R. Niu, J. B. Surya, J.-Z. Zhang, C.-H. Dong, G.-C. Guo, H. X. Tang, C.-L. Zou, *Opt. Lett.* **2019**, *44*, 1150.
[28] Y. N. Martinez de Escobar, S. Palacios Álvarez, S. Coop, T. Vanderbruggen, K. T. Kaczmarek, M. W. Mitchell, *Opt. Lett.* **2015**, *40*, 4731.
[29] L. Stern, J. R. Stone, S. Kang, D. C. Cole, M. Suh, C. Fredrick, Z. Newman, K. Vahala, J. Kitching, S. A. Diddams, S. B. Papp, *Sci. Adv.* **2020**, *6*, eaax6230.
[30] P. Balling, M. Fischer, P. Kubina, R. Holzwarth, *Opt. Express* **2005**, *13*, 9196.
[31] W. C. Swann, S. L. Gilbert, *J. Opt. Soc. Am. B* **2005**, *22*, 1749.
[32] M. Triches, M. Michieletto, J. Hald, J. K. Lyngsø, J. Lægsgaard, O. Bang, *Opt. Express* **2015**, *23*, 11227.
[33] M. Takiguchi, Y. Yoshikawa, T. Yamamoto, K. Nakayama, T. Kuga, *Opt. Lett.* **2011**, *36*, 1254.
[34] K. Knabe, S. Wu, J. Lim, K. A. Tillman, P. S. Light, F. Couny, N. Wheeler, R. Thapa, A. M. Jones, J. W. Nicholson, B. R. Washburn, F. Benabid, K. L. Corwin, *Opt. Express* **2009**, *17*, 16017.
[35] L. Tombez, E. J. Zhang, J. S. Orcutt, S. Kamlapurkar, W. M. J. Green, *Optica* **2017**, *4*, 1322.
[36] C. Philippe, R. Le Tragat, D. Holleville, M. Lours, T. Minh-Pham, J. Hrabina, F. Du Burck, P. Wolf, O. Acef, in 2016 European Frequency Time Forum, IEEE, Piscataway, NJ **2016**, p. 1.
[37] J. W. Hahn, Y. S. Yoo, J. Y. Lee, J. W. Kim, H.-W. Lee, *Appl. Opt.* **1999**, *38*, 1859.
[38] I. Goykhman, B. Desiatov, J. Khurgin, J. Shappir, U. Levy, *Opt. Express* **2012**, *20*, 28594.
[39] I. Goykhman, B. Desiatov, S. Ben-Ezra, J. Shappir, U. Levy, *Opt. Express* **2013**, *21*, 19518.
[40] M. H. Idjadi, F. Aflatouni, *Nat. Commun.* **2017**, *8*, 1.
[41] A. Pasquazi, M. Peccianti, L. Razzari, D. J. Moss, S. Coen, M. Erkintalo, Y. K. Chembo, T. Hansson, S. Wabnitz, P. Del'Haye, X. Xue, A. M. Weiner, R. Morandotti, *Phys. Rep.* **2018**, *729*, 1.
[42] R. Zektzer, L. Stern, N. Mazurski, U. Levy, *Appl. Phys. Lett.* **2016**, *109*, 10.
[43] A. Stamminger, J. Ettl, J. Grosse, M. Hörschgen-Eggers, W. Jung, A. Kallenbach, G. Raith, W. Saedtler, S. Seidel, J. Turner, M. Wittkamp, in *Proc. 22nd ESA Symp. Eur. Rocket Balloon Program and Related. Research*, ESA, Tromsϕ, Norwegen, **2015**, pp. 183–190.
[44] J. Williams, S. Chiow, N. Yu, H. Müller, *New J. Phys.* **2016**, *18*, 025018.
[45] V. Schkolnik, K. Döringshoff, F. B. Gutsch, M. Oswald, T. Schuldt, C. Braxmaier, M. Lezius, R. Holzwarth, C. Kürbis, A. Bawamia, M. Krutzik, A. Peters, *EPJ Quantum Technol.* **2017**, *4*, 9.
[46] L. Stern, B. Desiatov, N. Mazurski, U. Levy, *Nat. Commun.* **2017**, *8*, 14461.
[47] E. Talker, P. Arora, Y. Barash, L. Stern, U. Levy, *ACS Photonics* **2018**, *5*, 2609.
[48] F. Benabid, F. Couny, J. C. Knight, T. A. Birks, P. S. J. Russell, *Nature* **2005**, , *434*, 488.
[49] S. Ghosh, J. E. Sharping, D. G. Ouzounov, A. L. Gaeta, *Phys. Rev. Lett.* **2005**, *94*, 1.
[50] F. Benabid, P. Light, F. Couny, P. Russell, *Opt. Express* **2005**, *13*, 5694.
[51] H. Lee, M. G. Suh, T. Chen, J. Li, S. A. Diddams, K. J. Vahala, *Nat. Commun.* **2013**, *4*, 2468.
[52] V. Mahal, A. Arie, *Appl. Opt.* **1996**, *35*, 3010.
[53] X. Lu, G. Moille, Q. Li, D. A. Westly, A. Singh, A. Rao, S.-P. Yu, T. C. Briles, S. B. Papp, K. Srinivasan, *Nat. Photonics* **2019**, *13*, 593.
[54] M. Ducloy, *Phys. Rev. A* **1988**, *38*, 5197.
[55] W. C. Swann, S. L. Gilbert, *J. Opt. Soc. Am. B* **2000**, *17*, 1263.
[56] S. L. Gilbert, W. C. Swann, *Nist Spec. Publ.* **2001**, 133.
[57] J. L. Hall, *Science* **1978**, *202*, 147.
[58] K. Ikeda, R. E. Saperstein, N. Alic, Y. Fainman, *Opt. Express* **2008**, *16*, 12987.
[59] J. Vanier, C. Mandache, *Appl. Phys. B* **2007**, , *87*, 565.
[60] A. Naiman, B. Desiatov, L. Stern, N. Mazurski, J. Shappir, U. Levy, *Opt. Lett.* **2015**, *40*, 1892.
[61] X. Ji, F. A. S. Barbosa, S. P. Roberts, A. Dutt, J. Cardenas, Y. Okawachi, A. Bryant, A. L. Gaeta, M. Lipson, *Optica* **2017**, *4*, 619.
[62] H. Lee, M. G. Suh, T. Chen, J. Li, S. A. Diddams, K. J. Vahala, *Nat. Commun.* **2013**, *4*, 6.
[63] J. Hald, L. Nielsen, J. C. Petersen, P. Varming, J. E. Pedersen, *Opt. Express* **2011**, *19*, 2052.